OPEN ACCESS

Performances of Nano-Structured Cu_2O Thin Films Electrochemically Deposited on ITO Substrates in Lactate Bath as Liquid Petroleum Gas Sensors

To cite this article: A. H. M. N. N. Bandara *et al* 2023 *ECS Adv.* **2** 046501

ECS Advances, 2023 **2** 046501

Performances of Nano-Structured Cu_2O Thin Films Electrochemically Deposited on ITO Substrates in Lactate Bath as Liquid Petroleum Gas Sensors

A. H. M. N. N. Bandara,[z] V. P. S. Perera,[z] G. K. R Senadeera,[z] and K. N. D Bandara[z]

Department of Physics, Faculty of Natural Sciences, The Open University of Sri Lanka, Sri Lanka

The investigations are focused on structural and surface morphological features and their influence on electrical and wetting characteristics against liquid petroleum gas (LPG) sensing of synthesized nanostructured cuprous oxide (Cu_2O) thin films grown by electrochemical deposition (ECD) on indium tin oxide (ITO) glass substrates in lactate bath (pH 10). p-Cu_2O films revealed a cubical-tetrahedron nano-scale polycrystalline grain distribution (average grain size: 64.2 nm, inter planer spacing: 0.24 nm) that exhibited dominance in the crystallographic plane (111). LPG sensing evaluations of p-Cu_2O/ITO done at 70 °C constant temperature with 100% LPG at 5 cc min^{-1} flow rate, showed excellent gas sensor response, recovery, and stability over time due to its moderate wetting behavior (average contact angle: ~86°). AC impedance measurements carried out at room temperature demonstrated an ionic to electronic conduction variation from 100 Hz to 1 MHz, due to adsorption/desorption of LPG molecules (C_nH_{2n+2}) and oxygen species on the nano-particles surface. Cu_2O/ITO flat band potential was found to be higher than its' ambient state after exposure to LPG with an increment in acceptor density. Overall, this efficient LPG sensing could be attributed to the interfacial properties of Cu_2O thin films and ITO substrates, that provide an optimized fabrication process of nano-structured Cu_2O thin films.

 [DOI: 10.1149/2754-2734/ad040a]

Manuscript submitted December 14, 2022; revised manuscript received March 7, 2023. Published October 31, 2023.

Early detection and monitoring of flammable, toxic, and exhaust gases used in industrial and domestic environments such as Liquid Petroleum Gas (LPG) demands gas sensors of higher selectivity and sensitivity with a suitable base material consisting of ideal surface and bulk properties. Solid-state gas sensor development has been pursued in semiconducting, thermal conducting, electrochemical, catalytic combustion, and other techniques by past research. Here Semiconductor Metal Oxide (SMO) is one of the most investigated materials used as gas sensors due to their advantages in structural and morphological features. Recent studies on SMO focus on less than 100 nm particle size range to emerge unique electrical and chemical properties for enhanced sensing.[1] And also about how their geometry affects the movement of electrons and holes in these semiconductor nanomaterials.

Most of the SMO sensing materials are crystalline in nature. Their adjacent grains are interconnected by necks and form larger aggregates connected by grain boundaries. At ambient sensor conditions, ionosorbtion[2,3] takes place at SMO surfaces by absorbing oxygen in the air and driving the adsorbed oxygen molecules to trap surface electrons in the conduction band of SMO. As a result, O_2, O^{-} and O^{2-} are generated at the surface under relevant temperatures as given in Eqs. 1–4

$$O_2(g) \rightarrow O_2(ads) \quad [1]$$

$$O_2(ads) + e^- \rightarrow O_2^-(ads) \quad [2]$$

$$O_2^-(ads) + e^- \rightarrow 2O^- \quad [3]$$

$$O^- + e^- \rightarrow O^{2-} \quad [4]$$

This electron-depleted surface charge region (space charge layer) creates a potential barrier at the surface.[4] In polycrystalline sensing materials, electronic conduction happens via grain-to-grain contacts depending on the potential barrier of adjacent grains called the Schottky barrier.[5]

Based on the type of conductivity of the SMO surface layer, carrier concentration gets increased or decreased. A potential barrier induced by the decrease in major carrier (electron) concentration increases n-type SMO resistance. On the other hand, p-type SMO displays reducing resistance with the formation of active oxygen species, which strengthens the hole concentration by trapping electrons from the surface. When a reducing gas such as LPG is introduced to the ionosorbed oxygen molecules on n-type SMO films, the surface-trapped electrons get released. This decreases the film sensor resistance.[5] Figure 1 schematically shows this LPG sensing mechanism of p-Cu_2O thin films deposited on ITO substrates.

Literature reports, among the semiconducting metal oxides like SnO_2, In_2O_3, Fe_2O_3, ZnO, WO_3, TiO_2, Cu_2O, V_2O_5, CuO, etc.[6–19] Cuprous Oxide (Cu_2O) is an ideal material for researches due to its advantageous in non-toxicity, mechanical, electrical, and catalytic properties and the natural abundance of the base material.[20–28] At present, a variety of techniques exist to synthesize Cu_2O with different microstructures on selected substrates, including thermal oxidation with copper sheets at 200 °C/1050 °C, chemical vapor deposition with alumina slides at 300 °C, magnetron DC sputtering on glass at 693 K, radio, anodic oxidation on glass at 280 °C[29–33] etc. However, in many respects, such as ease of film fabrication and low cost, low processing temperature, controlled crystallization with surface morphology, roughness, and wettability in a large area, high deposition rate,[34] Cu_2O thin films produced by electrochemical deposition are highly suitable for gas sensors, solar cells, photo-electrochemical cells, and catalytic applications. Most of the said metal-oxide gas sensors perform at high temperatures. Since only limited works have been done in low temperature operated gas sensors, identifying the other variables affecting gas sensitivity has been a major challenge. For these reasons, this work reports the conditions for the successful deposition of Cu_2O nanostructured thin films on Indium Tin Oxide (ITO) substrates by electrodeposition technique, emphasizing structural, morphological, wettability and electrical features and their influence in LP gas sensing at low operating temperatures.

Experimental

Electrochemical deposition of nanostructured Cu_2O films.— Before the deposition of Cu_2O films, ITO substrates were subjected to surface treatment with an acetone bath and sonicated for several minutes with distilled water to improve Cu_2O film adhesion to the ITO surface. Selection of the potentiostatic conditions and deposition

[z]E-mail: doneranji@gmail.com; vpper@ou.ac.lk; gksen@ou.ac.lk; knban@ou.ac.lk

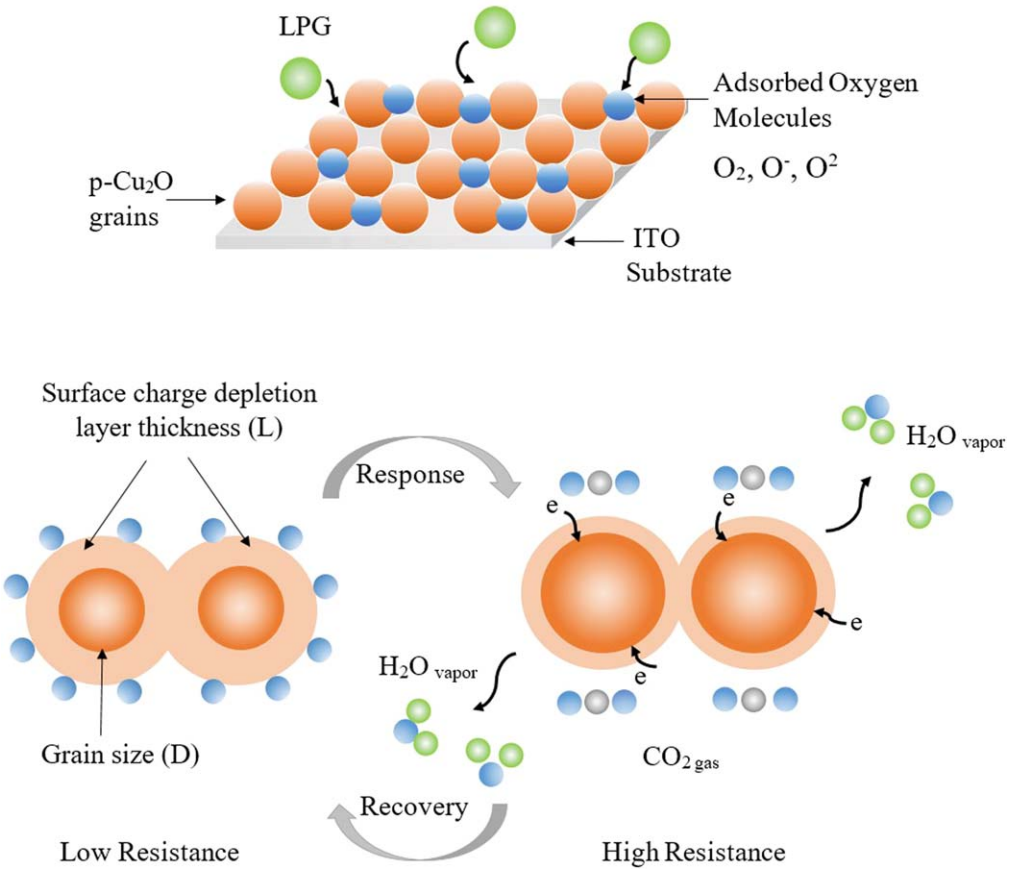

Figure 1. Schematic interpretation of semiconductor metal oxide LP gas sensing mechanism.

period also depends on the substrates' characteristics. During the electrodeposition, an area of $\sim 1 \times 1\ cm^2$ of the ITO substrate was immersed in an electrolyte solution containing 3.5 M lactic acid (Sigma–Aldrich, purity − 99.0%) and 0.45 M cupric sulfate $CuSO_4$ (Sigma–Aldrich, purity − 99.0%). The pH of the electrolyte was brought to pH 10 using 4 M NaOH (Sigma–Aldrich, purity—98.0%). Applied deposition time varies from 45–60 min with the thickness of the ITO to obtain a particular thickness of the Cu_2O film. The Cu_2O thin films were potentiostatically electrodeposited on an ITO glass in a lactate bath at −450 mV versus Ag/AgCl reference electrode in a three-electrode electrochemical cell with a platinum plate as the counter electrode for 45 min.[16] Here the electrolyte temperature was maintained constant by continuing the deposition in a water bath at 60 °C. After deposition, films were thoroughly cleaned with distilled water and allowed to dry in air at room temperature.[35]

Cu_2O thin film characterization.—The phase of cuprous oxide and the average crystal size were monitored using the X-ray Diffraction (XRD) (Regaku Ultima–IV) operating at 40 kV and 30 mA tube voltage and current with Cu-Kα ($\lambda = 1.5418$ Å) as the source of X- rays in the 20°−80° 2Θ range. The significant effect of the film grain size on the sensitivity and conductance of Cu_2O films and the inter-planer spacing (d) between the particles can be analyzed by considering the diffraction peaks observed with the XRD analysis by Debye–Scherrer formula and Braggs law given in Eqs. 5–6. Where "λ" is the wavelength of X-ray (0.1541 nm), "β" is the FWHM (full width at half maximum) of the prominent peak, "θ" is the diffraction angle corresponding to the peak, and "D" is the mean grain diameter size of the film.

$$D = \frac{0.9 \quad \lambda}{\beta \cos\theta} \qquad [5]$$

$$2d \quad \sin\theta = n\lambda \qquad [6]$$

$$d = \frac{\lambda}{2 \quad \sin \quad \theta} \quad (n = 1)$$

The surface structure and morphology of deposited Cu_2O thin films were observed using a Scanning Electron Microscope (SEM) (Zeiss EVO 15 lS). The type of conductivity of the deposited Cu_2O films was verified using spectral response measurements and Motts-Schottky plots. An AUTOLAB Model PGSTAT 302 potentiostat/galvanostat was used to conduct Mott-Schottky analysis using three electrode chemical cell containing Cu_2O deposited ITO substrate as the working electrode, platinum counter electrode, and Ag/AgCl reference electrode in aqueous 0.1 mol L^{-1} sodium acetate solution as supporting electrolyte. Mott-Schottky and Electrochemical impedance spectroscopic (EIS) analysis were done by varying the voltage −0.5 V to 1.5 V and frequency 1 Hz–0.1 MHz respectively at both stages before and after introducing the electrochemically deposited Cu_2O thin film for LP gas sensing. The sessile drop method with double distilled water (parts of 5 μl) was used to measure the contact angles of the film at ambient atmospheric conditions. A digital microscope (2MP 1000x 8 LED USB Digital Microscope Endoscope) focused on the film contacting surface obtained an average contact angle of three separate distilled water droplets after allowing them to settle on the film surface for ~10 min.[35]

LP gas response measurements.—Gold-plated contact probes placed 1 cm apart on the film surface with optimal contact pressure measure the electrical resistance variation of the Cu_2O film with and without LPG. Film temperature was maintained constant by

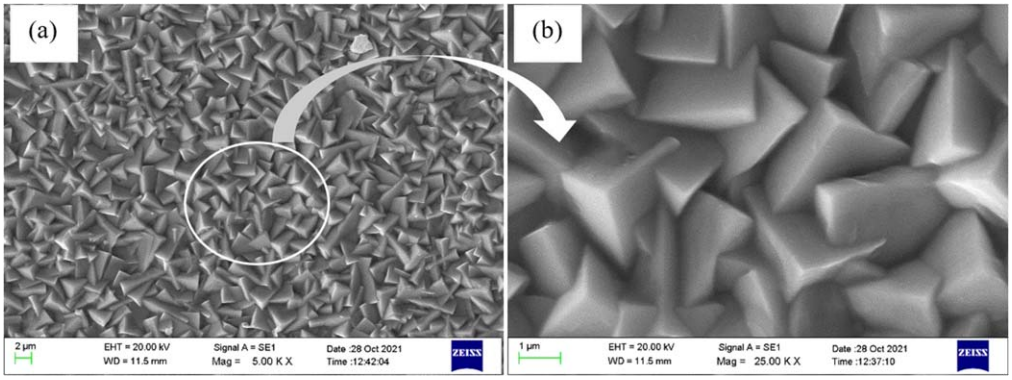

Figure 2. SEM morphological variations of electrodeposited Cu_2O (pH 10) thin films grown on ITO substrates in different magnifications.

mounting the films on a heating platform inside a stainless steel gas perfusion chamber. The thermocouple on the bare end of the substrate monitored the sensing temperature, ensuring zero leakage of LPG. The output electrical resistance of the film was processed using a computer interfaced Dual measurement multimeter (GW INSTEK GDM-9060/9061) at 2 s time intervals.[35] At the beginning of each measurement, the sample chamber was flushed with Nitrogen air, and the substrate was allowed to stabilize at the optimal temperature of 70 °C. At this point, thin film resistance (Ra) was stabilized in its ambient state. Next, LPG was introduced till the resistance reached a steady state maximum. Both resistance levels were measured with ±0.01 tolerance. With 100% LPG exposure, this variation takes typically 30–40 s duration. Finally, the gas flow was stopped to let the thin film recover its ambient state. Gases were applied through blue silica gel as a humidity-controlling measure to avoid external moisture getting inside the sealed chamber via valves.

Results and Discussion

Surface morphology and nano-crystal structure.—The operating characteristics of solid-state gas sensors depend on both receptor and transducer functions.[2] Semiconductor metal oxides with considerably small grain sizes and porous nature provide optimal surface morphology for such applications. Figures 2a–2b illustrate the top view of SEM micrographs obtained for the ITO/Cu_2O thin films electrochemically deposited for 45 min to get the optimum film thickness in this study. The Cu_2O surface has a well-defined grain distribution in nano-scale with considerably homogeneous, cubical-tetrahedron crystals. The surface adhesive nature of ITO has contributed to a pinhole-free compact nanostructured Cu_2O polycrystalline morphology that creates a large contacting surface area for adsorbed analytes. This crystallographic structure facilitates more surface oxygen vacancies for the diffusion of LPG, which improves the kinetics of the chemical reaction on the p-Cu_2O surface and shows possible enhanced gas sensing recovery.[4] In Fig. 3, the XRD patterns of p-Cu_2O (pH 10) films electrodeposited on ITO substrates in an aqueous electrolyte solution of 3.5 M lactic acid and 0.45 M cupric sulfate, at a constant temperature of 60 °C for 45 min duration is shown. The presented peaks corresponding to crystalline planes of (110), (111), (200), (220), and (311) are tallying with the standard JCPDS card PDF file no. 05–0667, which confirms the observed thin films to consist of Cu_2O nanoparticles. The crystallographic plane (111) is dominant in the acquired p-Cu_2O thin films influenced by ITOs' conductivity. The presence of relatively low peak intensities of (110), (200), (220), and (311) Cu_2O planes result in a polycrystalline nature in the observed thin films. This clarifies the cubical-tetrahedron grain distribution in Fig. 2.

Cu_2O Grain size and adhesive film nature.—The electrical conductance and gas sensitivity of the Cu_2O film have a significant dependency on its average grain size. A smaller grain size results in

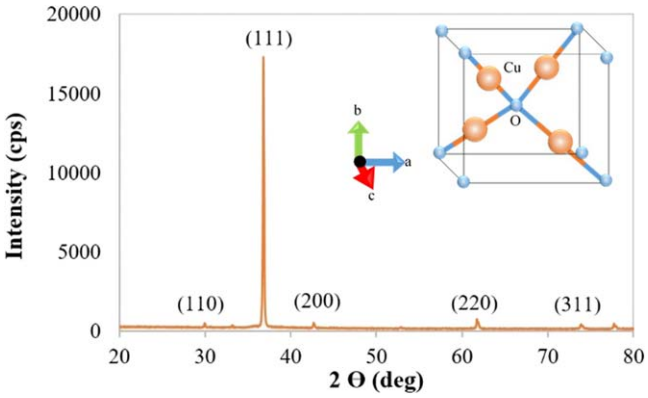

Figure 3. X-ray diffraction (XRD) spectra of (pH 10) Cu_2O thin films electrodeposited on ITO substrates. Inset illustrates the (111) crystallographic plane dominating cubic structure in Cu_2O.

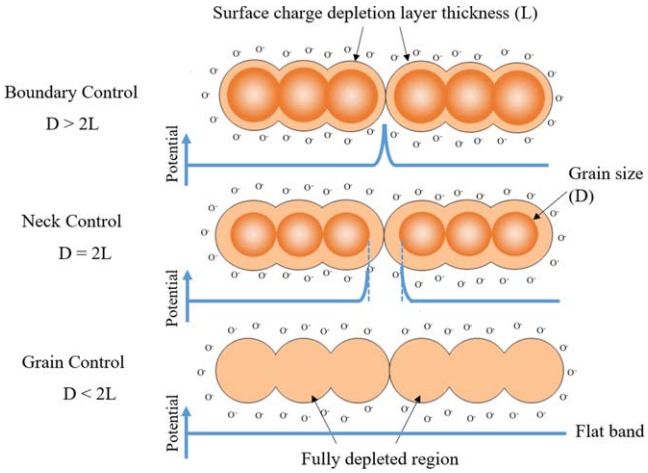

Figure 4. Grain size effect on conductance models of p-Cu_2O thin film grown on ITO.

high sensitivity, but a significant reduction in grain size decreases the structural stability of the film due to the small crystallites' deleterious nature on the temporal stability of the sensing platform.[35] The size dependence of gas sensitivity is explained by V. E. Bochenkov and G. B. Sergeev.[3] Recent studies on the gas sensitivity of nanostructured metal oxides[2–4] suggest a visible increase when the grain size D < 2 L, where L is the thickness of the surface charge layer. This is attributed to the higher grain contribution in creating the space charge layer causing the film conduction via grain

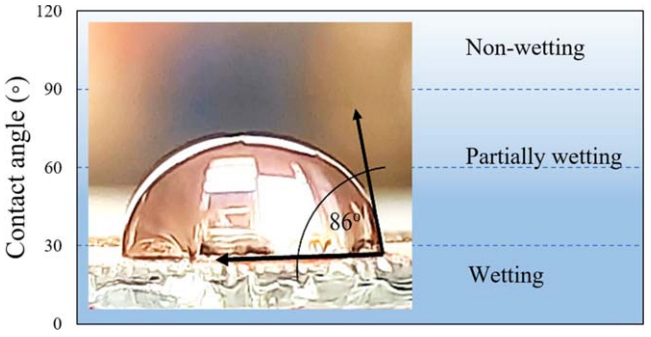

Figure 5. Average contact angle of electrodeposited Cu_2O (pH 10) thin films grown ITO substrates in lactate bath.

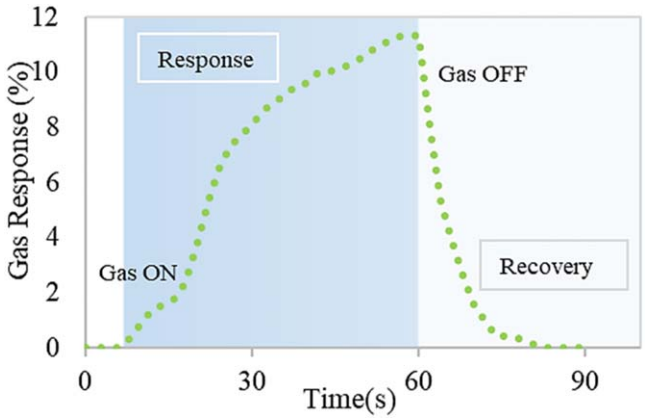

Figure 6. LPG response variation of electrodeposited Cu_2O (pH 10) thin films grown ITO substrates in lactate bath.

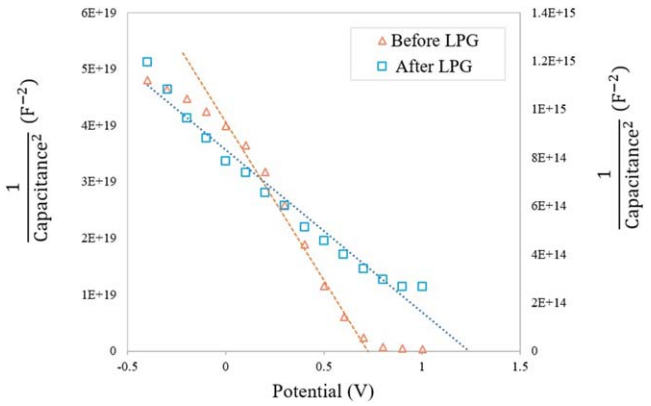

Figure 7. The linear regions of Mott-Schottky plots were observed for a selected Cu_2O (pH 10) thin film grown ITO substrates before and after it was introduced to LPG.

boundaries, grain necks, and grains itself (Fig. 4). Table I explains the grain size (D) and d-spacing calculations of each p-Cu_2O hkl plane observed in the thin films deposited on ITO substrates. The identified smaller average grain size of ∼64 nm drives a possible higher resistance response and gas sensitivity based on electronic conduction models observed in Fig. 9 with the semicircles presented.

Average contact angle, grain size variation, and the corresponding surface energy evaluate a thin film's wetting nature. The average contact angles measured for p-Cu_2O thin films deposited on ITO substrates have shown the probability of stable partially wetting behaviors according to the contact angle variations presented in former

Table I. Grain size and d-spacing calculations of p-Cu_2O thin films deposited on ITO substrates.

hkl plane	Grain size D (nm)	d-spacing (nm)
(110)	64.4	0.298
(111)	64.2	0.244
(200)	59.3	0.211
(220)	38.4	0.150
(311)	27.0	0.128

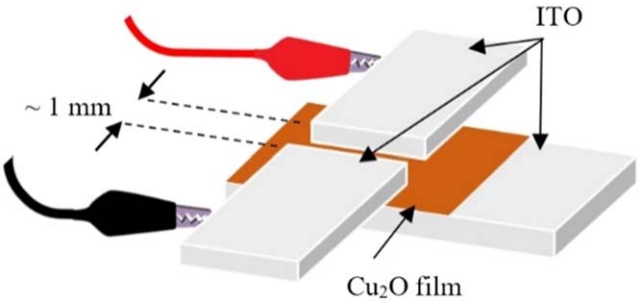

Figure 8. Schematic view of the impedance measurement across Cu_2O film surface deposited on ITO.

studies.[36] Figure 5 shows the average contact angle measurement of electrodeposited Cu_2O (pH 10) thin films grown on ITO substrates.

LPG sensing performance.—The resistance variations of the Cu_2O films electrochemically deposited on ITO were measured at ambient atmospheric conditions (Ra) and in the presence of 5 cc min^{-1} 100% LPG (Rg) concentration (Fig. 6). The time taken by the sensor to reach 90% of its maximum resistance response with LPG and to recover 90% of the ambient resistance were recorded. Upon the adsorption of LPG molecules on the film surface, the pre-stable resistance (∼0.1 MΩ at 70 °C) of the film increased and came to a saturation after a few seconds (30–40 s). But as it can be seen with the steeper slope in the line, film recovery is faster than the response at 70 °C. The percentage change in the gas response is given by Eq. 7. For p-type Cu_2O films Rg > Ra.

$$S = \left[\frac{(Rg - Ra)}{Ra}\right] \times 100\% \qquad [7]$$

Effect of LP exposure on carrier density.—A semiconductor material that perfectly abides by the Mott-Schottky plots can be characterized according to Eq. 8 below.

$$\frac{1}{C^2} = \left(\frac{2}{e\epsilon_0\epsilon_r N_D A^2}\right)\left(V - V_{FB} - \frac{kT}{e}\right) \qquad [8]$$

Where C, e, ϵ_0, ϵ_r, N_D, A, V_{FB}, k, and T are the space charge layer capacitance of the film at potential V, the electron charge, permittivity of the free space, the relative permittivity of Cu_2O free carrier concentration of the semiconductor, flat band potential, Boltzmann constant, and absolute temperature respectively. The Mott-Schottky analysis defines the conductivity type of electrochemically deposited Cu_2O thin films having negative slopes to be with p-type conductivity. The linear regions of Mott-Schottky plots observed for a selected Cu_2O film, before and after it was introduced to LPG, are illustrated in Fig. 7. Referring to the plots, flat band potential (V_{FB}) and the free carrier concentration[37,38] has been calculated using the following simplifications of Eq. 8.

Table II. Flat band potentials and carrier densities of Cu_2O thin films deposited on ITO substrates before and after LPG exposure.

LPG status	Conductivity	Flat band potential	Free carrier concentration
Before LPG	p-type	0.72 V	6×10^{17}
After LPG	p-type	0.97 V	3×10^{22}

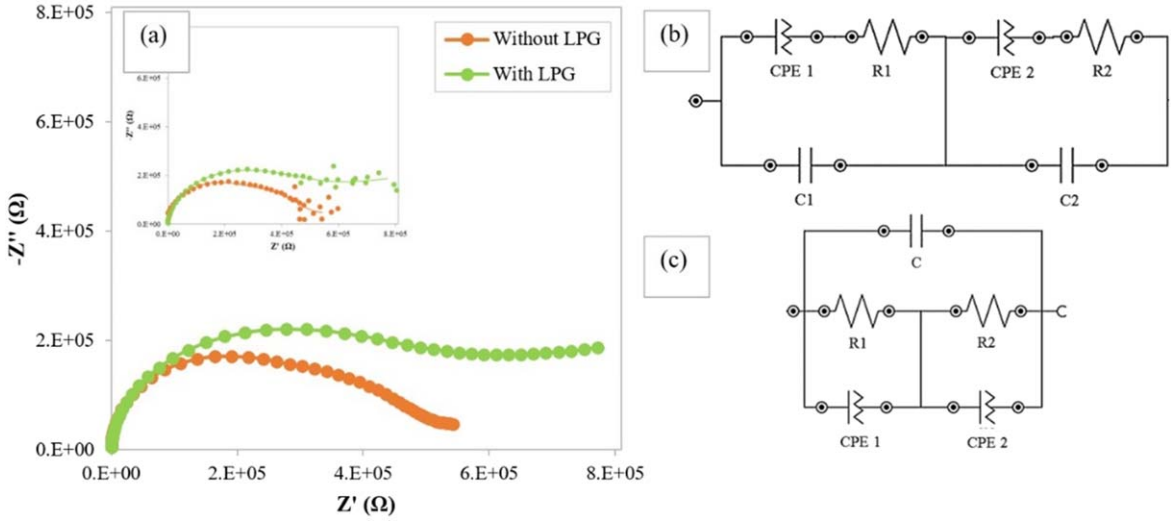

Figure 9. (a) Comparison of complex plane impedance plots of p-Cu_2O thin film grown on ITO and respective equivalent circuits simulated (b) without LPG and (c) with LPG. Inset of (a) gives the corresponding experimental and the fit and simulated impedance curves (given in solid lines).

$$N_D = \left(\frac{2}{e\epsilon_0\epsilon_r A^2(\text{slope})} \right) \quad [9]$$

$$V_{FB} = -\left(\frac{\text{intercept}}{\text{slope}} + \frac{kT}{e} \right) \quad [10]$$

The obtained flat band potentials (V_{FB}) and the free carrier concentrations measurements both before and after LPG exposure are listed in Table II. The LPG exposure time was limited to ~2 min at room temperature (300 K). In both instances, Cu_2O thin film on ITO shows a p-type conductivity with holes as the major carriers. The flat band potential of Cu_2O film after exposure to LPG once is higher than its original state. But the LPG interaction has drastically increased the free carrier density of a 1 cm^2 area.

When LPG is introduced, the interaction of hydrocarbons (C_nH_{2n+2}) and chemisorbed oxygen increases the adsorption rate of the film surface. The given additional pressure produces gaseous species and H_2O as a result (Eq. 11).

$$O^{2-} + C_nH_{2n+2} \rightarrow CO_2 + H_2O + 2e^- \quad [11]$$

Since the p-Cu_2O layer deposited on ITO shows low wettability, formed water molecules depart and create a potential barrier.[39] At high temperatures (180 °C), these water molecules are removed from the surface thereby, decreasing sensor resistance back to its original state. This water vapor concentration and pressure are high at low operating temperatures (70 °C). Therefore an increase in resistance in the Cu_2O film can be observed with LPG.

Electrical characteristics by EIS.—The electrical properties such as concentration of electroactive species, charge transfer, adsorption and diffusion of species, mass transfer of p-Cu_2O/ITO interface, and the film could be observed via EIS measurements by monitoring the current response to an AC voltage. These features are characterized by a fit and simulated equivalent electrical circuit to the measured impedance spectra, which consists of resistors, capacitors, constant phase elements (CPE), etc, that are connected in series or parallel. Figure 8 schematically shows the impedance measurement across the Cu_2O film surface deposited on ITO. Due to the difference in the electrical response rate of each component on the microscopic time scale, it is not reliable to measure impedance by a DC method.[39–43] Here in the EIS measurement, the Nyquist plot interprets the imaginary component Z'' versus the real component Z'

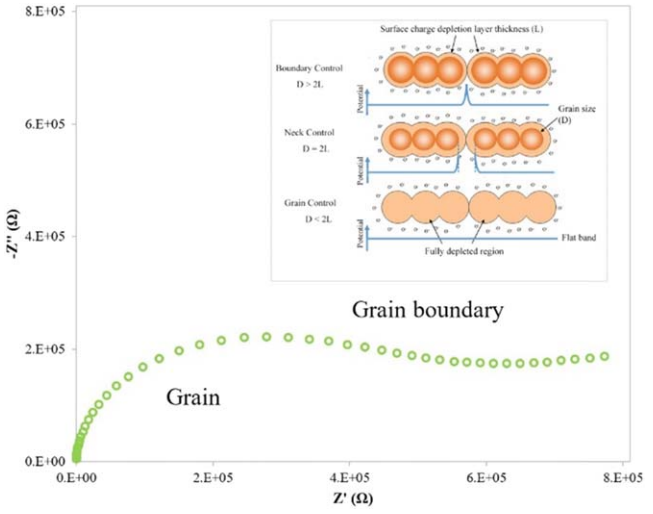

Figure 10. Complex plane impedance plot corresponding to the grain effect and conductance models (given in inset) of p-Cu_2O thin film grown on ITO exposed to LPG.

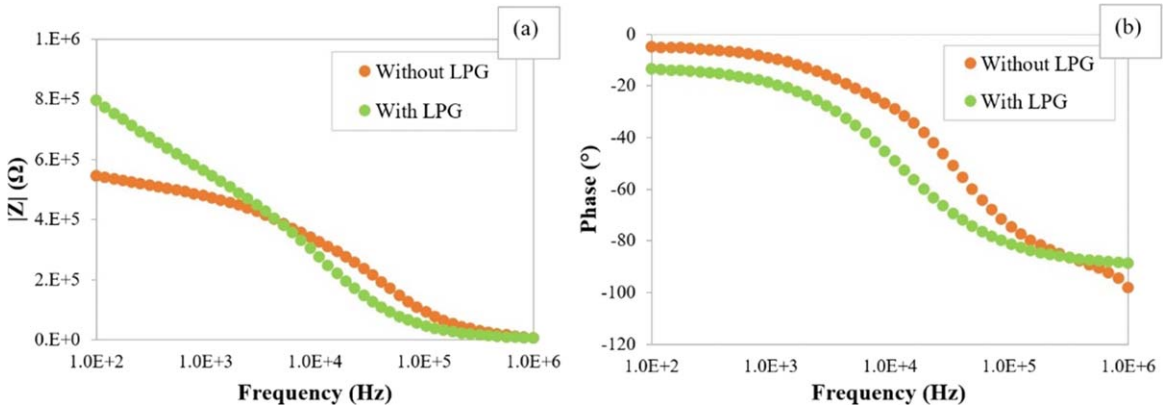

Figure 11. Comparison of (a) Bode impedance magnitude plots and (b) Bode phase plots observed for a selected Cu_2O (pH 10) thin film grown on ITO with and without it was introduced to LPG.

of the total impedance of the film for different frequencies. The bode plot gives the impedance modulus |Z| and phase angle variations versus frequency.

AC Impedance spectroscopy study was carried out in 100 Hz to 1 MHz frequency range with an oscillating voltage amplitude (V_{RMS}) of 10 mV within a current range of 10 nA to 100 mA at room temperature. Nyquist and bode plots were obtained for the process under zero forward bias DC voltage. Impedance measurements were taken across the film surface by placing two identical Fluorine Doped Tin Oxide (FTO) substrates contacting the film surface with their conducting sides. The gap between the FTOs was kept at ∼1 mm distance, with equal proportions of the FTOs on the film. However, longer the distance, the film cannot flow a smaller current across the film surface, resulting in a distorted impedance spectrum. As the figure inset explains, impedance response is weaker in low frequencies and way more consistent and strong in higher frequencies due to white noise. Figure 9a shows the Nyquist plot of the p-Cu_2O under normal atmospheric conditions and while it was introduced to a 5 cc min^{-1} LPG flow rate for 1–2 min duration at room temperature. During the AC impedance measurement, the surface roughness variations and non-homogeneity in the deposited polycrystalline p-Cu_2O film furnish a double-layer capacitance having non-ideal capacitive behavior.[45] Radius of the non-centered deformed semicircles on the Z' axis implies the total impedance of the film to be increased with the exposure of LPG from low (right) to high (left) frequencies. This explains the observed reducing electronic conductivity (Fig. 6) of the p-Cu_2O film surface with the LPG adsorption at room temperature. Moreover, the diffusion/adsorption of species causes the impedance and capacitance of the film in the low-frequency range, reporting ionic conduction of H^+ and OH^- ions on the p-Cu_2O film surface.[42–44] However, the film reaches a pure resistive state within this range without LPG contact. The equivalent circuit models of the film at both stages of LPG are represented in Figs. 9b, 9c show reasonable concordance with these simulated results.

Here, R_S (∼0) is the series resistance of the ohmic contacts between the film surface and FTO. The combination of parallel circuits at both LPG stages represents the deformation of the semicircular arks to the start of second semi-circles. As discussed earlier, grain size impact on film conductance is clearly visible with LPG, which exhibited two arcs at low and high frequencies corresponding to the grain and grain boundary effects, respectively.[3] The corresponding conductance models are illustrated in Fig. 10. Without LPG the film behaves as a parallel connection of capacitances (C_1 and C_2) formed with series connections of charge transfer resistance components (R_1 and R_2) and constant phase elements (CPE_1 and CPE_2). But with LPG, constant phase elements are in parallel with R_1 and R_2.

The significant impedance modulus in Fig. 11a, and negative phase angles observed in Fig. 11b, at high frequency ranges of p-Cu_2O/ITO films exposed to LPG are associated with a capacitive nature which lessens at lower frequencies, thereby revealing a resistive nature and almost zero phase change corresponding to the ionic conduction of H^+ and OH^- ions on the p-Cu_2O film surface. The discussed pure resistive state of the film in the absence of diffusion ions resulted in an LPG response (Fig. 8) can be identified with the increasing phase angle reaching a zero in Fig. 11b.

Conclusions

In summary, Cu_2O electrochemically deposited on ITO has a grain distribution in nano-scale with considerably homogeneous and cubical tetrahedron crystals. The surface adhesive nature of ITO has contributed to a pinhole-free compact nano-structured Cu_2O polycrystalline morphology that creates a large contacting surface area for adsorbed analytes exhibiting promising LP gas sensitivity and enhanced gas sensing recovery. Evidence supporting the explanation of these measurements was further clarified by the contact angle measurement and resulting partial wetting nature. The characterized film was subjected to gas sensing evaluations at a constant temperature of 70 °C which ultimately confirmed that ITO can improve gas sensor performances with their moderate wetting behaviors. Under stable sensing conditions, Cu_2O/ITO exhibited enhanced LPG response, recovery, and stability over time. After the exposure to LPG, the films' flat band potential and acceptor density of a 1 cm^2 area were identified to be higher than their original state. AC impedance spectroscopy was carried out at room temperature. With the diffusion/adsorption of LPG species at room temperature impedance characteristics were recorded to vary from ionic to electronic conduction on the p-Cu_2O film surface from low to high frequencies. In comparison, all the experimental results highlighted the impact of LPG on the interfacial properties of Cu_2O thin films deposited on ITO substrates.

ORCID

A. H. M. N. N. Bandara https://orcid.org/0000-0001-7286-7939
G. K. R Senadeera https://orcid.org/0000-0002-9202-9008

References

1. G. Korotcenkov, "Metal oxides for solid-state gas sensors: What determines our choice?" *Mater. Sci. and Eng.: B*, **139**, 1 (2007).
2. X. F. Wang, X. Z. Song, K. M. Sun, L. Cheng, and W. Ma, "MOFs-derived porous nanomaterials for gas sensing." *Polyhedron*, **152**, 155 (2018).
3. Bochenkov and G. B. Sergeev, "Sensitivity, selectivity, and stability of gas-sensitive metal-oxide nanostructures." *Metal Oxide Nanostructures and their Applications*, ed. Ahmad and Y.B. Hahn (American Scientific Publishers, Moscow, Russia) 3, 31 (2010).
4. M. S. Choi, M. Y. Kim, A. Mirzaei, H. S. Kim, S. I. Kim, S. H. Baek, D. W. Chun, C. Jin, and K. H. Lee, "Selective, sensitive, and stable NO2 gas sensor based on porous ZnO nanosheets." *Appl. Surf. Sci.*, **568**, 150910 (2021).
5. K. N. D. Bandara, K. M. D. C. Jayathilaka, M. S. Gunewardene, D. P. Dissanayake, and J. K. D. S. Jayanetti, "Surface properties of sulphur based surface modified n-Cu2O thin films for enhanced liquefied petroleum gas sensing." *J. Phys. D: Appl. Phys.*, **50**, 485304 (2017).

6. G. B. Barbi, J. P. Santos, P. Serrini, P. N. Gibson, M. C. Horrillo, and L. Manes, "Ultrafine grain-size tin-oxide films for carbon monoxide monitoring in urban environments." *Sens. Actuators, B*, **25**, 559 (1995).
7. G. Han, Q. Lu, G. Liu, X. Ye, S. Lin, Y. Song, B. Liu, X. Yang, and G. Li, "Enhanced ethanol sensing properties based on α-Fe_2O_3/In $_2O_3$ hollow microspheres." *J. Mater. Sci., Mater. Electron.*, **23**, 1616 (2012).
8. S. Zhang, F. Ren, W. Wu, J. Zhou, X. Xiao, L. Sun, Y. Liu, and C. Jiang, "Controllable synthesis of recyclable core–shell γ-Fe $_2O$ $_3$ &SnO_2 hollow nanoparticles with enhanced photocatalytic and gas sensing properties." *PCCP*, **15**, 8228 (2013).
9. J. Xu, Q. Pan, and Z. Tian, "Grain size control and gas sensing properties of ZnO gas sensor." *Sens. Actuators, B*, **66**, 277 (2000).
10. D. Barreca, E. Comini, A. P. Ferrucci, A. Gasparotto, C. Maccato, C. Maragno, G. Sberveglieri, and E. Tondello, "First example of ZnO− TiO_2 nanocomposites by chemical vapor deposition: structure, morphology, composition, and gas sensing performances." *Chem. Mater.*, **19**, 5642 (2007).
11. Y. K. Chung, M. H. Kim, W. S. Um, H. S. Lee, J. K. Song, S. C. Choi, K. M. Yi, M. J. Lee, and K. W. Chung, "Gas sensing properties of WO3 thick film for NO_2 gas dependent on process condition." *Sens. Actuators, B*, **60**, 49 (1999).
12. P. Murugan, R. D. Nagarajan, A. K. Sundramoorthy, D. Ganapathy, R. Atchudan, D. Nallaswamy, and A. Khosla, "Electrochemical detection of H2O2 Using an activated glassy carbon electrode." *ECS Sens. Plus*, **1**, 034401 (2022).
13. T. Hyodo, W. Sakata, T. Ueda, and Y. Shimizu, "Effects of surface modification of platinum electrodes with gold on hydrogen-sensing properties of diode-type sensors." *ECS Sens. Plus*, **1**, 013602 (2022).
14. T. Ueda, N. Oide, K. Kamada, T. Hyodo, and Y. Shimizu, "Improved toluene response of mixed-potential type YSZ-Based gas sensors using CeO2-Added Au electrodes." *ECS Sens. Plus*, **1**, 013604 (2022).
15. P. Manusha, K. Theyagarajan, M. Elancheziyan, H. Shankar, K. Thenmozhi, and S. Senthilkumar, "Anthraquinone functionalized ionic liquid based disposable electrochemical sensor for the enzyme-free detection of hydrogen peroxide." *ECS Sens. Plus*, **1**, 033601 (2022).
16. B. K. Miremadi, R. C. Singh, Z. Chen, S. R. Morrison, and K. Colbow, "Chromium oxide gas sensors for the detection of hydrogen, oxygen and nitrogen oxide." *Sens. Actuators, B*, **21**, 1 (1994).
17. D. Patil, P. Patil, V. Subramanian, P. A. Joy, and H. S. Potdar, "Highly sensitive and fast responding CO sensor based on Co_3O_4 nanorods." *Talanta*, **81**, 37 (2010).
18. M. Yu, X. Liu, Y. Wang, Y. Zheng, J. Zhang, M. Li, W. Lan, and Q. Su, "Gas sensing properties of p-type semiconducting vanadium oxide nanotubes." *Appl. Surf. Sci.*, **258**, 9554 (2012).
19. L. Liao et al., "Multifunctional CuO nanowire devices: p-type field effect transistors and CO gas sensors." *Nanotechnol.*, **20**, 085203 (2009).
20. W. Siripala and K. P. Kumara, "A photoelectrochemical investigation of the n-and p-type semiconducting behaviour of copper (I) oxide films." *Semicond. Sci. Technol.*, **4**, 465 (1989).
21. W. Siripala, K. M. D. C. Jayathileka, and J. K. D. S. Jayanetti, "Low cost solar cells with electrodeposited cuprous oxide." *J. Bionanosci.*, **3**, 118 2 (2009).
22. A. H. Jayatissa, P. Samarasekara, and G. Kun, "Methane gas sensor application of cuprous oxide synthesized by thermal oxidation." *physica status solidi (a)*, **206**, 332 (2009).
23. J. L. K. Jayasingha, K. M. D. C. Jayathilaka, M. S. Gunewardene, D. P. Dissanayake, and J. K. D. S. Jayanetti, "Electrodeposited n-type cuprous oxide cubic nanostructures for liquefied petroleum gas sensing." *physica status solidi (b)*, **254**, 1600333 (2017).
24. D. Barreca, E. Comini, A. Gasparotto, C. Maccato, C. Sada, G. Sberveglieri, and E. Tondello, "Chemical vapor deposition of copper oxide films and entangled quasi-1D nanoarchitectures as innovative gas sensors." *Sens. Actuators, B*, **141**, 270 (2009).
25. F. S. B. Kafi, R. P. Wijesundera, and W. Siripala, "Enhanced Photoelectrochemical Water Splitting by Surface Modified Electrodeposited n-Cu2O Thin Films." *physica status solidi (a)*, **217**, 2000330 (2020).
26. F. S. B. Kafi, K. M. D. C. Jayathileka, R. P. Wijesundera, and W. Siripala, "Effect of Bath pH on Interfacial Properties of Electrodeposited n-Cu2O Films." *physica status solidi (b)*, **255**, 1700541 (2018).
27. K. M. D. C. Jayathilaka, V. Kapaklis, W. Siripala, and J. K. D. S. Jayanetti, "Surface treatment of electrodeposited n-type Cu2O thin films for applications in Cu2O based devices." *physica status solidi (RRL)*, **8**, 592 (2014).
28. L. Wan, D. Cheng, and P. Wang, "Synthesis of cuprous oxides thin film with different morphologies by electrodeposition, In 2015 International Power." *Electronics and Materials Engineering Conference* (Atlantis Press) 1182 (2015).
29. A. O. Musa, T. Akomolafe, and M. J. Carter, "Production of cuprous oxide, a solar cell material, by thermal oxidation and a study of its physical and electrical properties." *Sol. Energy Mater. Sol. Cells*, **51**, 305 (1998).
30. S. Dolai, S. Das, S. Hussain, R. Bhar, and A. K. Pal, "Cuprous oxide (Cu2O) thin films prepared by reactive dc sputtering technique." *Vacuum*, **141**, 296 (2017).
31. N. Saadaldin, M. N. Alsloum, and N. Hussains, "Preparing of copper oxides thin films by chemical bath deposition (CBD) for using in environmental application." *s. l.: Energy Procedia*, **74**, 1459 (2015).
32. A. M. Selman, M. A. Mahdi, and Z. Hassan, "Fabrication of Cu2O nanocrystalline thin films photosensor prepared by RF sputtering technique." *Physica E*, **94**, 132 (2017).
33. O. Sişman, N. Kılınç, and Z. Z. Öztürk, "H2 sensing properties of Cu2O nanowires on glass substrate." *Procedia Eng.*, **120**, 1170 (2015).
34. R. G. Ehl and A. J. Ihde, "Faraday's electrochemical laws and the determination of equivalent weights." *J. Chem. Educ.*, **31**, 226 (1954).
35. A. H. M. N. N. Bandara, V. P. S. Perera, G. K. R. Senadeera, and K. N. D. Bandara, "Substrate effect on liquid petroleum gas sensors of cuprous oxide thin films electrodeposited in acetate bath." *ECS J. Solid State Sci. Technol.*, **11**, 107002 (2022).
36. Y. L. Liu, Y. C. Liu, R. Mu, H. Yang, C. L. Shao, J. Y. Zhang, Y. M. Lu, D. Z. Shen, and X. W. Fan, "The structural and optical properties of Cu2O films electrodeposited on different substrates." *Semicond. Sci. Technol.*, **20**, 44 (2004).
37. A. A. Hssi, L. Atourki, N. Labchir, M. Ouafi, K. Abouabassi, A. Elfanaoui, A. Ihlal, and K. Bouabid, "Optical and dielectric properties of electrochemically deposited p-Cu2O films." *Mater. Res. Expres*, **7**, 016424 (2020).
38. C. F. Windisch Jr and G. J. Exarhos, "Mott–Schottky analysis of thin ZnO films." *J. Vacuum Sci.Tech. A*, **18**, 1677 (2000).
39. V. Guidi, M. A. Butturi, M. C. Carotta, B. Cavicchi, M. Ferroni, C. Malagu, G. Martinelli, D. Vincenzi, M. Sacerdoti, and M. Zen, "Gas sensing through thick film technology." *Sens. Actuators*, B**84**, 72 (2002).
40. S. H. Magar, R. Y. A. Hassan, and A. Mulchandani, "Electrochemical impedance spectroscopy (EIS): Principles, construction, and biosensing applications." *Sensors*, **21**, 6578 (2021).
41. T. Kuwabara, Y. Kawahara, T. Yamaguchi, and K. Takahashi, "Characterization of inverted-type organic solar cells with a ZnO layer as the electron collection electrode by ac impedance spectroscopy." *ACS Appl. Mater. Interfaces*, **1**, 2107 (2009).
42. L. Manjakkal, K. Cvejin, J. Kulawik, K. Zaraska, D. Szwagierczak, and G. Stojanovic, "Sensing mechanism of RuO2–SnO2 thick film pH sensors studied by potentiometric method and electrochemical impedance spectroscopy." *J. Electroanal. Chem.*, **759**, 82 (2015).
43. A. Lasia, "Electrochemical impedance spectroscopy and its applications." *Modern Aspects of Electrochemistry* (Springer, Boston, MA) 143 (2002).
44. P. Das, B. Mondal, and K. Mukherjee, "Simultaneous adsorption–desorption processes in the conductance transient of anatase titania for sensing ethanol, a distinctive feature with kinetic perception." *J. Phys. Chem.*, **121**, 1146 (2017).